Bio-Sensing by Mach–Zehnder Interferometer Comprising Doubly-Corrugated Spoofed Surface Plasmon Polariton (DC-SSPP) Waveguide

Zhao Xu and Pinaki Mazumder, *Fellow, IEEE*

Abstract—The paper describes the design and analysis of a Mach-Zehnder interferometer (MZI) structure consisting of doubly-corrugated spoofed surface plasmon polariton (DC-SSPP) waveguide. The dependence of phase change on the dielectric loading of the DC-SSPP structure causes the output from both arms to interfere and enhances features on the transmission spectrum of the MZI. The paper uses a mathematical model to predict the phase accumulation of THz signals travelling through each arm of the MZI with various sample loadings. HFSS simulation has been performed to verify the theoretical modeling and produce more sophisticated results. The paper demonstrates that compared with single-armed SSPP waveguide, the proposed MZI structure shows significant shift of the transmission maxima and minima with high quality factors for the transmission peaks when different materials are loaded. The paper also demonstrates that the proposed DC-SSPP MZI structure can be potentially used in tag-free bio-molecular sensing. The highly localized $E-M$ field at frequencies close to SSPP resonance is shown to reduce the sample amount needed to produce interference patterns without affecting the selectivity of the sensing structure.

Index Terms—Bio-molecular sensing, doubly-corrugated spoofed surface plasmon polariton (DC-SSPP), Mach–Zehnder interferometer (MZI), phase difference.

I. INTRODUCTION

TERAHERTZ elements and devices designed to work in the frequency range of 0.1–10 THz have attracted enormous research activities in the past decade or so due to its potential use in applications such as astronomical remote sensing, tag-free bio-molecular detection, and monitoring of harmful chemicals [1]–[4]. Intensive studies on the generation, transmission and detection mechanisms of THz signals also demonstrated the possibility of building integrated circuits in THz frequency range, which is known to have broader bandwidth than the operating frequency range of the current-generation VLSI devices and circuits [5]–[8]. A major hurdle encountered by designers of THz logic components is how to realize low-loss and low-dispersion transmission of electromagnetic signals. One way to overcome the problem is to introduce periodic surface features such as holes, grooves, and dimples onto the material interface of the structure, which generates a special surface mode known as the Spoofed Surface Plasmon Polariton (SSPP) [9]–[11]. Such pseudo mode mimics the common optical surface plasmon mode traveling at dielectric-metal interface, and therefore has a similar mode profile with strongly confined $E-M$ field and localized energy distribution [12]–[15].

By introducing one-dimensional (1-D) periodic grooves on opposite interfaces of metal-dielectric-metal waveguides, we realized the doubly-corrugated SSPP (DC-SSPP) structure. Our previous work provided extensive theoretical study along with computer simulations to demonstrate the existence of discrete transmission bands as well as SSPP modes with close-to-zero group velocity in such DC-SSPP structures [7], [15]. It has also been shown that the spectral response of DC-SSPP structures strongly depends on the geometrical dimensions and the choice of building materials. As a result, a number of passive and active SSPP components such as frequency filters and Boolean switches have been proposed and the related research work has been reported in other publications from our group [7], [15], [16].

A common issue in the design of THz components is to achieve better spectral selectivity in the form of sharper transmission peaks. Higher sensitivity to the structural change caused by external stimuli is also preferred in the design of sensors and active components alike. Song *et al.* has proposed the Waveguide-Cavity-Waveguide structure on top of the DC-SSPP design, which has provided a quality factor of $Q \sim 700$ for its transmission peaks. With such high-Q factor, a binary switching of state can be triggered by slightly modulating (~ 0.01) the refractive index of the dielectric material [16]. In this paper, we propose an interferometer design which combines two arms of the DC-SSPP structure together to form a Mach-Zehnder interferometer (MZI). While the MZI structure is often used in other scenarios to realize signal controls based on phase delay, with the help of DC-SSPP structure this structure is applied to the THz frequency domain.

The paper is organized as follows: In Section II a mathematical model is provided to characterize the phase shift of the DC-SSPP structure when loaded with different dielectric materials. In Section III computer simulations for different DC-SSPP MZI structures are carried out and the simulation data are analyzed. Discussions on the MZI structure and its applications in bio-sensing are provided in Section IV, followed by a brief conclusion in Section V.

The authors are with the Department of Electrical Engineering and Computer Science, University of Michigan, Ann Arbor, MI 48109 USA (e-mail: mazum@eecs.umich.edu).

II. THEORETIC ANALYSIS

The DC-SSPP structure under investigation is illustrated in Fig. 1. In order to derive the mathematical form of the dispersion relation, such structure is divided into two regions: Region I is the main waveguide cavity without corrugations, and Region II represents the periodic groove areas. Mirror symmetry of the structure dictates the modes to be either symmetric or anti-symmetric along the z-axis. The x-component of the mode, on the other hand, is best expressed by Floquet mode expansions due to the periodic nature of the waveguide. With these considerations, for the symmetric mode, the EM fields within the two regions (Region I and Region II) are expressed below [15].

In *Region I*:

$$\begin{bmatrix} H_x^{I} \\ H_y^{I} \\ H_z^{I} \end{bmatrix} = \sum_{n=-\infty}^{\infty} \rho_n e^{jk_{x,I}^{(n)}x} \begin{bmatrix} j\frac{k_y k_{x,I}^{(n)}}{v_y^2}\cos(k_y y)\cos\left(k_{z,I}^{(n)}z\right) \\ \sin(k_y y)\cos\left(k_{z,I}^{(n)}z\right) \\ -\frac{k_y k_{z,I}^{(n)}}{v_y^2}\cos(k_y y)\sin\left(k_{z,I}^{(n)}z\right) \end{bmatrix} \quad (1)$$

$$\begin{bmatrix} E_x^{I} \\ E_y^{I} \\ E_z^{I} \end{bmatrix} = \frac{1}{\omega\epsilon}\frac{k_0^2}{v_y^2}\sum_{n=-\infty}^{\infty}\rho_n e^{jk_{x,I}^{(n)}x}$$
$$\times \sin(k_y y)\begin{bmatrix} jk_{z,I}^{(n)}\sin\left(k_{z,I}^{(n)}z\right) \\ 0 \\ -k_{x,I}^{(n)}\cos\left(k_{z,I}^{(n)}z\right) \end{bmatrix}. \quad (2)$$

In *Region II*:

$$\begin{bmatrix} H_x^{II} \\ H_y^{II} \\ H_z^{II} \end{bmatrix} =$$
$$\begin{bmatrix} -\frac{k_y k_{x,II}}{v_y^2}(A^+ e^{jk_{z,II}z} + A^- e^{-jk_{z,II}z})\cos(k_y y)\sin(k_{x,II}x) \\ (A^+ e^{jk_{z,II}z} + A^- e^{-jk_{z,II}z})\sin(k_y y)\cos(k_{x,II}x) \\ j\frac{k_y k_{z,II}}{v_y^2}(A^+ e^{jk_{z,II}z} - A^- e^{-jk_{z,II}z})\cos(k_y y)\cos(k_{x,II}x) \end{bmatrix} \quad (3)$$

$$\begin{bmatrix} E_x^{II} \\ E_y^{II} \\ E_z^{II} \end{bmatrix} = \frac{1}{\omega\epsilon}\frac{k_0^2}{v_y^2}\sin(k_y y)$$
$$\times \begin{bmatrix} k_{z,II}(A^+ e^{jk_{z,II}z} - A^- e^{-jk_{z,II}z})\cos(k_{x,II}x) \\ 0 \\ -jk_{x,II}(A^+ e^{jk_{z,II}z} + A^- e^{-jk_{z,II}z})\sin(k_{x,II}x) \end{bmatrix}. \quad (4)$$

In the above descriptions, a, d, h, t, W are different geometrical dimensions of the structure, as shown in Fig. 1. $k_{x,j}^{(n)}$ and $k_{z,j}^{(n)}$ denote the wavevectors of the nth-order Floquet mode along x- and z-axis in Region I, and ρ_n signifies its amplitude coefficient. Correspondingly, $k_{x,II}$ and $k_{z,II}$ denote the wave vectors along the two axis in Region II. Other variables are defined as follows:

$$v_y^2 = k_0^2 - k_y^2 = \left(k_{x,I}^{(n)}\right)^2 + \left(k_{z,I}^{(n)}\right)^2 \text{ in Region I}$$
$$v_y^2 = k_0^2 - k_y^2 = k_{x,II}^2 + k_{z,II}^2 \text{ in Region II}$$
$$k_y = \frac{m\pi}{W}, \qquad m = 1, 2, \ldots$$
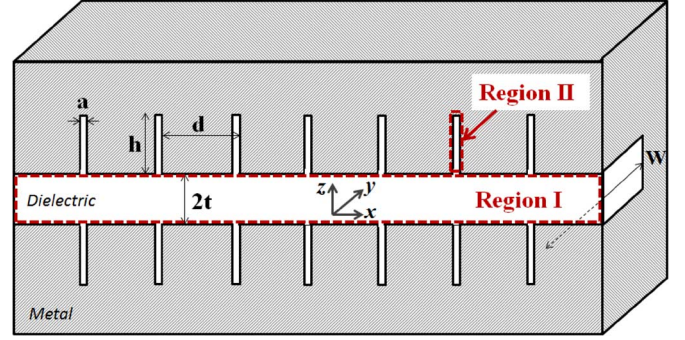$$k_{x,II} = \frac{l\pi}{a}, \qquad l = 0, 1, 2, \ldots$$

Fig. 1. Cross section of the single-armed DC-SSPP structure with different geometric dimensions labeled. W is the width of the waveguide along the y-direction. The structure can be divided into Regions I and II as shown.

Across the boundary between Regions I and II, the E–M fields must be continuous. By equating E_x and H_y in the two regions and integrate both sides of the two equations along one period of the structure, we have the following equation:

$$-j\sum_{n=-\infty}^{\infty}\frac{k_{z,II}}{k_{z,I}^{(n)}}\frac{|T_n|^2}{\tan\left(k_{z,I}^{(n)}t\right)}(B^+ - B^-) = (B^+ + B^-) \quad (5)$$

where

$$|T_n|^2 = \left|\sqrt{\frac{1}{ad}}\int_0^a e^{jk_{x,I}^{(n)}x}dx\right|^2 = \frac{a}{d}\left|\text{sinc}\left(\frac{k_{x,I}^{(n)}}{2}a\right)\right|^2 \quad (6)$$

$$B^+ = A^+ e^{jk_{z,II}t}, \qquad B^- = A^- e^{-jk_{z,II}t}. \quad (7)$$

The tangential E field must vanish at the bottom of the groove. Therefore we have, from (4)

$$B^+ e^{jk_{z,II}h} - B^- e^{-ijk_{z,II}h} = 0. \quad (8)$$

By combining (5) and (8), a matrix equation for $[B^+, B^-]^T$ is obtained. For it to have non-trivial solutions, the determinant of the matrix must be zero. The dispersion relation can be hence obtained as below:

$$1 + \sum_{n=-\infty}^{\infty}\frac{k_{z,II}}{k_{z,I}^{(n)}}\frac{|T_n|^2}{\tan\left(k_{z,I}^{(n)}t\right)}\tan(k_{z,II}h) = 0 \quad (9)$$

Following a similar procedure, the dispersion relation of the anti-symmetric mode can be derived to be:

$$1 - \sum_{n=-\infty}^{\infty}\frac{k_{z,II}}{k_{z,I}^{(n)}}|T_n|^2\tan\left(k_{z,I}^{(n)}t\right)\tan(k_{z,II}h) = 0 \quad (10)$$

The wave vectors as mentioned above are functions of refractive index n of the dielectric material. Therefore, when a modulation on n is somehow introduced, it is possible to modulate the wave vector, hence the phase accumulation of the THz wave traveling within the structure. As an example, the dispersion relationship of one DC-SSPP structure ($d = 100 \ \mu m$, $a/d = 0.1$, $h/d = 0.8$, $t/d = 1/3$, $W = 300 \ \mu m$) calculated from (9) using MATLAB[1] is shown in Fig. 2 . The waveguide is made of dielectric materials having three different refractive indices $n_0 = 1$, $n_1 = 1.05$ and $n_2 = 1.15$. In the figure the dispersion

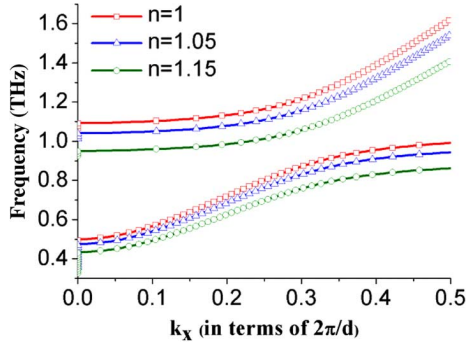[1]MATLAB, Mathworks Inc., Natick, MA.

Fig. 2. Dispersion relation of the single-armed DC-SSPP structure when filled with dielectric material of different refractive indices.
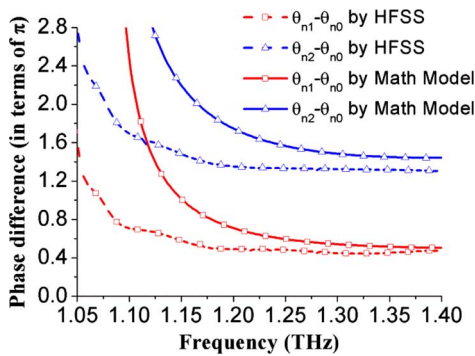

Fig. 3. Difference in phase accumulation for THz signals as a function of frequency between three refractive indices ($n_0 = 1$, $n_1 = 1.05$ and $n_2 = 1.15$), as obtained using the analytical model and HFSS simulations, respectively.

curve is seen to be significantly lowered when higher refractive index material is used.

A natural result of this modified dispersion relations is the difference in phase accumulations when the THz signals propagate through such DC-SSPP structures with different dielectric constant. In Fig. 3 we show the phase difference of THz signals after it travels through seven periods of the DC-SSPP waveguide with three refractive indices ($n_0 = 1$, $n_1 = 1.05$ and $n_2 = 1.15$). The solid lines represent the result obtained from our mathematical model and the dashed lines show the simulation results obtained using HFSS software[2] . It is observed that the two curves are close to each other with frequencies far from the SSPP resonance. Near the band-gap region, despite the observable disparities, both curves show a sharp increase of the phase difference, as is predicted from Fig. 2 with flattened dispersion curves.

The two curves have a diverging discrepancy near the band-gap, to which various reasons may apply. The main factor contributing to this difference is the *edge effect*, which signifies the distorted strong $E-M$ field around the edges of the grooves near resonance. Under such circumstance, the waveguide cannot be accurately described as the combination of the distinctive Region I and Region II, which can give rise to errors in the analytical calculation. Our previous works have studied the same

structure using both analytical models and CST simulation software [15].[3]. Between two approaches a difference of $\sim$0.07 THz in resonance frequency is demonstrated. Such number agrees with the results we obtained here.

Another basic difference in the two approaches is the assumption of an infinite waveguide in our mathematic model, whereas in HFSS simulation the structure must have a finite length in the propagation direction. To study the effect of the latter, we simulated similar structures with different number of periods up to 20 grooves. The results demonstrate close to linear change of the signal phase delay and no significant alleviation of the discrepancy with the increase in the waveguide length, therefore ruled out its contribution to such disparities. We will hence consider the SSPP waveguide with as few as 7 grooves to be effectively periodic, and will use it as the basic building block for our MZI structures throughout this paper.

Frequency filters as well as switches have been designed with single-armed DC-SSPP waveguide since it has been demonstrated to have frequency selective transmission curves. Such designs, however, only take advantage of the transmission selectivity of the DC-SSPP waveguide, and usually suffer from the broad peaks of their transmission curves before it can achieve better frequency resolution and sensitivity. When phase modulation by changing refractive index n is demonstrated as above, we can combine two arms of DC-SSPP waveguides to form an MZI. The THz signal from two arms of the MZI, when recombined after they propagate through different dielectric materials will be either enhanced or reduced in magnitude as a result of coherent interference. The combined effect of the selectivity of single-armed DC-SSPP waveguide and that of the interferometer will result in a transmission curve with sharper features as well as better sensitivity to structural variations caused by external modulations.

III. SIMULATION RESULT

In order to verify our idea, we have simulated the DC-SSPP MZI structure as depicted in Fig. 4. Various dimensions are labeled in the figure, with D denoting the distance between the two waveguide arms. The first structure we simulate has the dimensions of $d = 100$ μm, $a/d = 0.1$, $h/d = 0.8$, $t/d = 1/3$, $W = 300$ μm, and $D = 250$ μm, and each arm consists of a DC-SSPP waveguide with 7 grooves. With three different dielectric materials filling up one of the arms and air ($n_0 = 1$) filling up the rest of the structure, the transmission curves of the MZI are shown in Fig. 5(a). For comparison, the transmission curves of the single arm DC-SSPP structure of the same dimensions are shown in Fig. 5(b).

It is quite obvious that by introducing MZI structure on top of the DC-SSPP waveguide, the spectral features on the transmission curves are greatly enhanced. Above the first band-gap, single-armed waveguide barely shows any suppression of the transmitted signal beyond 5 dB, while the distinction between the pass and the stop bands of the MZI structure is quite significant. The peaks and valleys of the transmission curves of the single-armed waveguide, and those of the MZI structure with $n_0 = 1$ (i.e., when both arms are filled with air) come from the
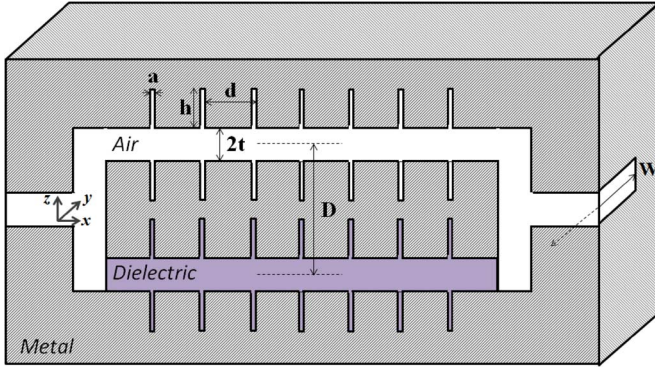
Fig. 4. Cross section of the DC-SSPP MZI structure with different geometric dimensions labeled. W is the width of the waveguide along the y-direction. The lower arm of the MZI structure (shaded in purple) designates the volume with dielectric loading.

Frequency	1.084THz	1.152THz	1.240THz	1.348THz
T when n=1	-0.03dB	-0.01dB	-0.03dB	-0.03dB
T when n=1.05	-10.25dB	0.00dB	-0.78dB	-3.79dB
$\Delta\phi$: n_1-n_0	0.824π	0.571π	0.486π	0.453π
T when n=1.15	-0.10dB	-6.20dB	-18.18dB	-15.11dB
$\Delta\phi$: n_2-n_0	1.873π	1.473π	1.334π	1.319π

in Table I, the transmission peaks and valleys do not correspond perfectly to integers of π in phase difference. We attribute this mismatching partly to the fact that the transverse mode profile from two arms of the MZI structure is different when different materials are loaded, therefore their maximum enhancement or cancellation is shifted from the frequency otherwise predicted. The more complicated geometry of the interferometer also contributes to the disparity, when mode deflection on the additional walls and material interfaces cannot be neglected. Nonetheless, in Fig. 3 if we compare the phase difference between two arms in the cases of $n_1 = 1.05$ and $n_2 = 1.15$ (lines with square and triangle markers respectively), an almost constant difference of π is observed. This is consistent with the simulation results that the transmission peaks and valleys in the two cases are almost always inversed.

In Fig. 6, we have included the E field distributions on the cross section of the structure at the frequency of $f = 1.084$ THz. The constructive/destructive interference between the two arms in difference cases can be clearly seen. It is noticed that for frequencies close to the SSPP resonance, the E–M field is greatly localized in the groove region of the structure. It is consistent with the theoretical analysis we did before, where a strongly confined energy distribution of the THz wave is predicted near resonance [15]. This property indicates the possibility of using less amount of dielectric loading to achieve the same selectivity of the structure, which will be discussed more in detail in Section IV.

The enhancement to the ON/OFF ratio is beneficial for switching and sensing applications. In addition, the MZI DC-SSPP structure can in general produce sharper transmission peaks, which are desired in high spectral resolution THz detector designs. To better illustrate this property, we did simulation on a second MZI DC-SSPP structure with dimensions of $d = 100\,\mu$m, $a/d = 0.1$, $h/d = 0.3$, $t/d = 1/3$, $W = 300\,\mu$m, and $D = 250\,\mu$m. In Fig. 7(a), we show the transmission spectrum of this structure obtained by HFSS simulations with a number of different dielectric material loadings. As an example, with $n = 1.05$ filling up one of the arms, the Q-factor for the first peak shown in the figure is estimated to be ~400 and that for the third peak to be ~1300. Such peaks with high quality factor can be used as frequency filters when the detection of narrow spectral features is desired for certain applications.

It is also noticed that in this case, for the first peak a complete shift from ON to OFF state, with a contrast of 15 dB at $f = 1.548$ THz, can be induced by a refractive index change of 0.04. If the third peak is considered, such switching of state with an extinction ratio exceeding 20 dB can be achieved for a refractive index change of merely 0.01 (for example, at $f = 1.612$ THz
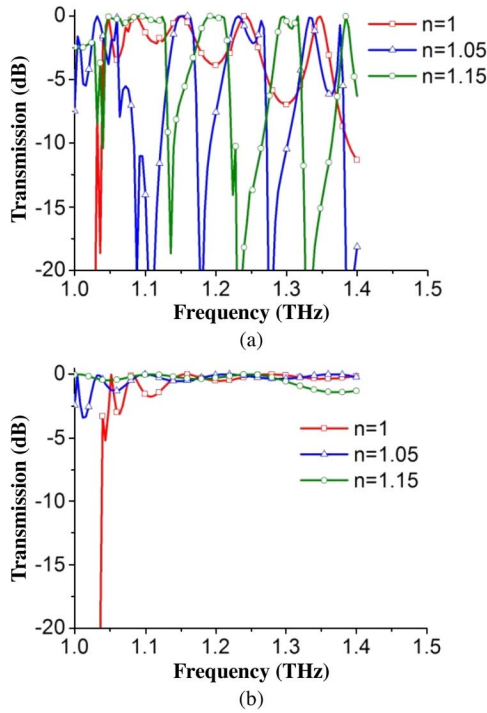

Fig. 5. Transmission spectrum of (a) the DC-SSPP MZI structure and (b) the single-armed DC-SSPP structure. Three different refractive indices are selected for the dielectric loading, and for MZI structure such loading only applies to one of the arms as depicted in Fig. 4.

Fabry-Perot etalon effect. While the F-P ripples are caused only by the periodicity of the grooves for the single-armed waveguide, for MZI structure they also come from multiple reflections from the walls that bounds the interferometer.

In Fig. 5(a), there are several frequencies where the MZI structure demonstrates distinct ON/OFF states when different dielectric materials are loaded. Some of those frequencies, along with the magnitude of transmission (T) and the phase difference, as predicted in Fig. 3, are listed in Table I.

By correlating the transmission with the phase difference, it is observed that significant suppression of the THz signal tends to happen when the phase difference between two arms of the interferometer is close to odd numbers of π. One may notice that
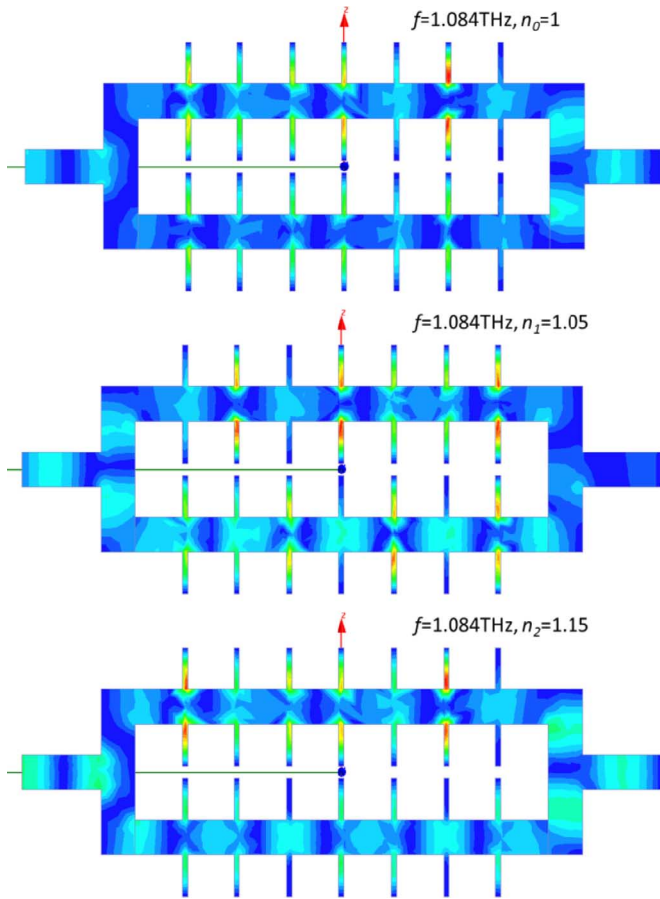
Fig. 6. An example of E field distribution in the DC-SSPP MZI structure at $f = 1.084$ THz for three different refractive indices (magnitude of the overall E field is plotted). The different dielectric loadings and frequencies are labeled on the upper right corner of each plot.
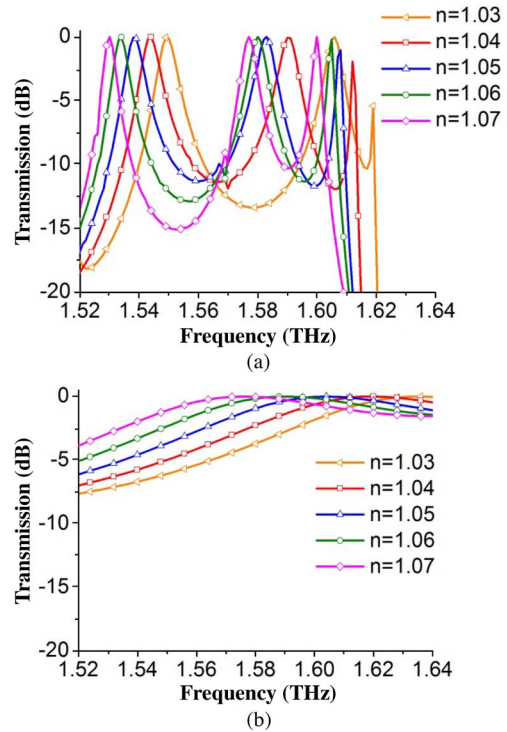

Fig. 7. Transmission spectrum of: (a) DC-SSPP MZI structure and (b) single-armed DC-SSPP structure. Five different refractive indices are selected as the dielectric loading, and for MZI structure such loading only applies to one of the arms as depicted in Fig. 4.

with $n = 1.05$ and $n = 1.06$). As a comparison, we have included the transmission curves for the single-armed waveguide with same dimensions in Fig. 7(b). Contrastingly, the flatness of those transmission spectra would prevent it from being useful in any frequency sensitive detector designs or THz switching components alike.

IV. APPLICATION AND DISCUSSION

When compared with the original design of a single-armed waveguide, the SSPP band-gap structure combined into an interferometer has resulted in sharper peaks in transmission curves, as well as higher sensitivity to refractive index changes of its dielectric loading. Those properties can be potentially applied to sensor designs. One example is the genetic diagnosis, usually referred to as the DNA biosensors, where the aim is to recognize the sequence of unknown polynucleotide by binding it with single-stranded "probe" DNA molecules with known sequences. The detection of the density of binding event is essential, since strong conjugation only happens between complementary base sequences.

Traditionally, the conformational change from the single-stranded ("denatured") DNA to the double-stranded ("hybridized") DNA molecules are tracked by tagging the target DNA with certain fluorescent agent [17]. Despite its

widespread use, this method suffers from numerous disadvantages such as the unwanted interference from the tagging agent, the fluorophore degradation and the extra preparatory steps, which are time consuming [18]–[20]. On the contrary, the hybridization event of DNA is shown to be able to shift the characteristic vibrational resonance (usually in THz frequencies) of the molecules, therefore inducing a change in its refractive index [4], [21], [22]. By detecting such refractive index change using probe THz beams, the intensity of hybridization can be quantitatively determined.

This idea of tag-free sensing of DNA molecules overcomes the disadvantages of the fluorescence-based sensing schemes, and has been shown to be effective. In some heraldic studies by other researchers, THz time domain spectroscopy (THz-TDS) is combined with various frequency selective structures in order to detect the spectral shift induced by the hybridization event. Those structures include planar and ring resonators made of thin-film microstrip lines (TFML) and SSPP waveguide with single-sided saw-tooth-shaped grooves [23]–[26]. In this paper, we propose to use the DC-SSPP MZI structure to detect directly the change in refractive index in the sample loading.

In the simulations we showed earlier, we intentionally selected the refractive indices of the dielectric loading to be $n_0 = 1$, $n_1 = 1.05$ and $n_2 = 1.15$. They represent the dielectric properties of air, denatured DNA and hybridized DNA respectively, according to previous experimental measurements of these samples in THz frequency domain [4]. As demonstrated earlier, the MZI structure produces transmission peaks that are quite distinguishable between the three dielectric loadings. By choosing
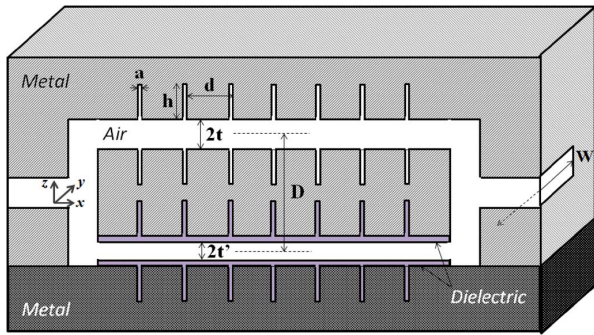
Fig. 8. Cross section of the DC-SSPP MZI structure with different geometric dimensions labeled. W is the width of the waveguide along the y-direction. Localized DNA loading is depicted as purple-shaded area in the sketch. The dark and light grey coloring of the metal part is merely to show the modular design of the sensor.
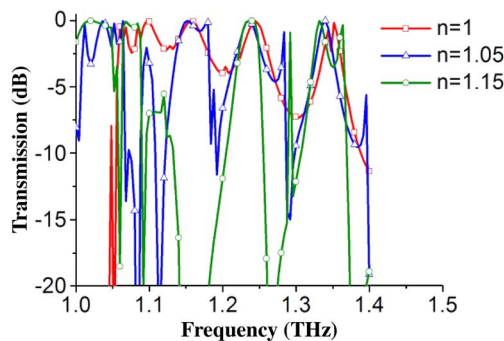

Fig. 9. The transmission spectrum of the DC-SSPP MZI structure with localized sample loadings. Three different refractive indices are selected as the dielectric loading, and for MZI structure such loading only applies to one of the arms.

TABLE II
TRANSMISSION (IN dB) AT SOME FREQUENCIES FOR THE DC-SSPP MZI STRUCTURE, WITH LOCALIZED LOADING OF DNA SAMPLES NEAR THE GROOVE REGION

Frequency	1.084THz	1.152THz	1.240THz	1.348THz
T when n=1	-0.35dB	-0.19dB	-0.24dB	-2.30dB
T when n=1.05	-39.2dB	0.00dB	-0.24dB	-1.71dB
T when n=1.15	-0.21dB	-21.36dB	0.00dB	-3.38dB

the right probe frequency, it is very straightforward to identify the different bio-molecules if they exist in the sample loadings.

The field distributions as shown in Fig. 6 demonstrate strong localization of the THz signal near the groove region of the structure, when the frequency is close to resonance. This indicates strong interaction of the dielectric material with the probe THz signal near the grooves. It is therefore possible to reduce the amount of sample usage without harming the sensitivity of the MZI structure, by localizing the DNA molecule loadings to the groove area. For that purpose we have simulated the MZI DC-SSPP structure with dimensions of $d = 100 \, \mu m$, $a/d = 0.1$, $h/d = 0.8$, $t/d = 1/3$, $W = 300 \, \mu m$, and $D = 250 \, \mu m$, this time with only the grooves plus a thin layer on each wall (with $t'/d = 0.2$) loaded with DNA samples (as shown in Fig. 8). The simulation result is shown in Fig. 9, and the magnitudes of transmission for the same set of frequencies are summed up in Table II.

From both Fig. 9 and Table II, it is observed that when the frequency is close to resonance ($f = 1.084$ THz and 1.152 THz for example), the difference in ON/OFF state as induced by different sample loadings still exists and is consistent with the cases in Table I. However with frequencies far away from the resonance, the difference in phase accumulation with different sample loadings will not be significant due to the delocalization of the E–M field, resulting in the mostly coinciding transmission peaks. This way, it is demonstrated that the spectral sensitivity of the MZI DC-SSPP structure to the refractive index change is not harmed by the localized loading of the dielectric sample near the groove region, should the probe frequency be close to the SSPP resonance. When compared with the full loading case, the amount of sample needed in this case can be reduced by as much as 50%.

In reality, the sensor based on MZI SSPP structure can be constructed with two modules as shown by the different shading of the metal part in Fig. 8. With the localized sample loading proved to be effective, the DNA preparation and immobilization process can be performed separately on the two modules of the sensor before they can be combined in a flip-chip manner and ready for test. Similar idea of the modular design has been implemented by other groups and its effectiveness has been demonstrated [27]. Such design is the key for disposable sensor constructions and can greatly reduce the running cost of the technique.

V. CONCLUSION

In this paper we have studied the MZI structure consisting of two arms of DC-SSPP waveguide. By combining the spectral response of the DC-SSPP structure and the interference effect of the MZI, the frequency selectivity is greatly enhanced in terms of both the ON/OFF switching ratio and the quality factor of the transmission peaks. Both mathematical modeling and elaborate simulation using HFSS software are shown to agree with each other reasonably well despite the existence of observable discrepancies near the SSPP resonance.

It is shown that the THz MZI DC-SSPP structure can be deployed in bio-molecular sensing. By using a probe THz beam with the correct frequency it is possible to distinguish between denatured DNA and hybridized DNA by detecting the change of their refractive indices. The strongly localized E-M field distribution of the structure also enables us to reduce the usage of bio-molecular samples. By depositing the sample loadings specifically near the groove region, the same spectral selectivity remains near the SSPP resonance frequency when compared with the fully-loaded case.

REFERENCES

[1] D. M. Mittleman, R. H. Jacobsen, and M. C. Nuss, "T-ray imaging," *IEEE J. Sel. Topics in Quantum Electron.*, vol. 2, pp. 679–692, 1996.

[2] P. H. Siegel, "Terahertz technology," *IEEE Trans. Microw. Theory Techn.*, vol. 50, no. 3, pp. 910–928, Mar. 2002.

[3] R. Kohler *et al.*, "Terahertz semiconductor-heterostructure laser," *Nature*, vol. 417, pp. 156–159, 2002.

[4] M. Brucherseifer, M. Nagel, P. Haring Bolivar, H. Kurz, A. Bosserhoff, and R. Büttner, "Label-free probing of the binding state of DNA by time-domain terahertz sensing," *Appl. Phys. Lett.*, vol. 77, no. 24, pp. 4049–4051, 2000.

[5] J. Tucek, D. Gallagher, K. Kreischer, and R. Mihailovich, "A compact, high power, 0.65 THz source," in *2008 IEEE Int. Vac. Electron. Conf. (IVEC 2008)*, 2008, pp. 16–17.

[6] Y.-M. Shin *et al.*, "Terahertz vacuum electronic circuits fabricated by UV lithographic molding and deep reactive ion etching," *Appl. Phys. Lett.*, vol. 95, p. 181505-3, 2009.

[7] K. Song and P. Mazumder, "Active terahertz spoof surface plasmon polariton switch comprising the perfect conductor metamaterial," *IEEE Trans. Electron Devices*, vol. 56, no. 11, pp. 2792–2799, Nov. 2009.

[8] H.-T. Chen, W. J. Padilla, J. M. O. Zide, S. R. Bank, A. C. Gossard, A. J. Taylor, and R. D. Averitt, "Ultrafast optical switching of terahertz metamaterials fabricated on ErAs/GaAs nanoisland superlattices," *Opt. Lett.*, vol. 32, no. 12, pp. 1620–1622, Jun. 2007.

[9] K. Wang and D. M. Mittleman, "Metal wires for terahertz wave guiding," *Nature*, vol. 432, pp. 376–379, 2004.

[10] J. B. Pendry, L. Martin-Moreno, and F. J. Garcia-Vidal, "Mimicking surface plasmons with structured surfaces," *Science*, vol. 305, pp. 847–848, Aug. 2004.

[11] W. Zhu, A. Agrawal, and A. Nahata, "Planar plasmonic terahertz guided-wave devices," *Opt. Express*, vol. 16, p. 6216, 2008.

[12] C. R. Williams, S. R. Andrews, S. A. Maier, A. I. Fperiodi-calernández-Domínguez, L. Martín-Moreno, and F. J. García-Vidal, "Highly confined guiding of terahertz surface plasmon polaritons on structured metal surfaces," *Nat. Photon.*, vol. 3, p. 175, 2008.

[13] A. I. Fernández-Domínguez, E. Moreno, L. Martín-Moreno, and F. J. García-Vidal, "Guiding terahertz waves along subwavelength channels," *Phys. Rev. B*, vol. 79, p. 233104, 2009.

[14] F. J. Garcia-Vidal, L. Martin-Moreno, T. W. Ebbesen, and L. Kuipers, "Light passing through subwavelength apertures," *Rev. Mod. Phys.*, vol. 82, pp. 729–787, 2010.

[15] Z. Xu, K. Song, and P. Mazumder, "Analysis of doubly corrugated spoof surface plasmon polariton (DC-SSPP) structure with sub-wavelength transmission at THz frequencies," *IEEE Trans. THz Sci. Technol.*, vol. 2, no. 3, pp. 345–354, May 2012.

[16] K. Song and P. Mazumder, "Dynamic terahertz spoof surface plasmon-polariton switch based on resonance and absorption," *IEEE Trans. Electron Devices*, vol. 58, no. 7, pp. 2172–2176, Jul. 2011.

[17] M. Chee, R. Yang, E. Hubbell, A. Berno, X. C. Huang, D. Stern, J. Winkler, D. J. Lockhart, M. S. Morris, and S. P. A. Fodor, "Accessing genetic information with high-density DNA arrays," *Science*, vol. 274, no. 25, pp. 610–614, Oct. 1996.

[18] H. Ozaki and L. W. McLaughlin, "The estimation of distances between specific backbone-labeled sites in DNA using fluorescence resonance energy-transfer," *Nucl. Acids Res.*, vol. 20, no. 19, pp. 5205–5214, Oct. 1992.

[19] Z. Zhu and A. S. Waggoner, "Molecular mechanism controlling the incorporation of fluorescent nucleotides into DNA by PCR," *Cytometry*, vol. 18, no. 3, pp. 206–211, Jul. 1997.

[20] M. L. Larramendy, W. El-Rifai, and S. Knuutila, "Comparison of fluorescein isothiocyanate- and Texas red-conjugated nucleotides for direct labeling in comparative genomic hybridization," *Cytometry*, vol. 31, no. 3, pp. 174–179, Mar. 1998.

[21] L. L. Van Zandt and V. K. Saxena, "Millimeter-microwave spectrum of DNA: Six predictions for spectroscopy," *Phys. Rev. A*, vol. 39, no. 5, pp. 2672–2674, Mar. 1989.

[22] W. Zhuang, Y. Feng, and E. W. Prohofsky, "Self-consistent calculation of localized DNA vibrational properties at a double-helix-single-strand junction with anharmonic potential," *Phys. Rev. A*, vol. 41, no. 12, pp. 7033–7042, 1990.

[23] M. Nagel, P. H. Bolivar, M. Brucherseifer, H. Kurz, A. Bosserhoff, and R. Buettner, "Integrated planar terahertz resonators for femtomolar sensitivity label-free detection of DNA hybridization," *Appl. Opt.*, vol. 41, no. 10, pp. 2074–2078, Apr. 2002.

[24] M. Nagel, F. Richter, P. Haring-Bolivar, and H. Kurz, "A functionalized THz sensor for marker-free DNA analysis," *Phys. Med. Biol.*, vol. 48, pp. 3625–3636, 2003.

[25] M. Nagel and H. Kurz, "Corrugated waveguide based genomic biochip for marker-free THz read-out," *Int. l J. Infrared Millim. Waves*, vol. 27, no. 4, pp. 517–529, April 2006.

[26] C. Debusa and P. H. Bolivar, "Frequency selective surfaces for high sensitivity terahertz sensing," *Appl. Phys. Lett.*, vol. 91, p. 184102, 2007.

[27] M. Nagel, M. Foerst, and H. Kurz, "THz biosensing devices: Fundamentals and technology," *J. Phys: Condens. Matter*, vol. 18, no. 18, pp. 610–618, 2006.

Zhao Xu received the B.S. degree in electronics engineering from Tsinghua University, Beijing, China, in 2006, and the M.S. degree in electrical engineering from the University of Michigan, Ann Arbor, in 2008, where he is currently working toward the Ph.D. degree.

He is a Graduate Student Research Assistant with the Electrical Engineering and Computer Science Department, University of Michigan, Ann Arbor. His current research interests include the modeling, simulation, and design of THz spoof plasmonic structures and components.

Pinaki Mazumder (F'99) received the Ph.D. degree from the University of Illinois at Urbana-Champaign, Urbana, in 1988.

He is currently a Professor with the Department of Electrical Engineering and Computer Science, University of Michigan (UM), Ann Arbor. He is currently on leave for one year from the UM to serve as the lead Program Director of the Emerging Models and Technologies Program with the U.S. National Science Foundation, Arlington, VA. He was for six years with industrial R&D centers that included AT&T Bell Laboratories, where in 1985, he started the CONES Project-the first C modeling-based very large scale integration (VLSI) synthesis tool at India's premier electronics company, Bharat Electronics, Ltd., where he developed several high-speed and high-voltage analog integrated circuits intended for consumer electronics products. His current research interests include current problems in nanoscale CMOS VLSI design, computer-aided design tools, and circuit designs for emerging technologies including quantum MOS and resonant tunneling devices, semiconductor memory systems, and physical synthesis of VLSI chips. He is the author or coauthor of more than 200 technical papers and four books on various aspects of VLSI research works.

Dr. Mazumder is a American Association for the Advancement of Science Fellow since 2008. He was a recipient of the Digital's Incentives for Excellence Award, BF Goodrich National Collegiate Invention Award, and Defense Advanced Research Projects Agency Research Excellence Award.